Chinese Journal of
POLYMER SCIENCE

RESEARCH ARTICLE

https://doi.org/10.1007/s10118-025-3366-y
Chinese J. Polym. Sci. **2025**, *43*, 1125–1133

Janus Particle Sizing Agent for Interfacial Enhancement of Basalt Fiber/Poly(vinyl chloride) Composites

Tian-Lin Liu[a], Peng Kang[b], Hui Wang[a,c], Da-Li Gao[b*], Kai Xu[b], Tao Cai[b], Qi Xin[b], Sheng-Peng Shi[b], Na Wang[c], and Fu-Xin Liang[a*]

[a] *Department of Chemical Engineering, Tsinghua University, Beijing 100084, China*
[b] *SINOPEC (Beijing) Research Institute of Chemical Industry Co., Ltd., Beijing 100013, China*
[c] *College of Materials Science and Engineering, Shenyang University of Chemical Technology, Shenyang 110142, China*

Abstract Sizing treatment is a suitable technique to modify the fiber-matrix interfaces without damage of inherent performance of fibers. In this work, sizing agents based on Janus particles (JPs) were utilized to enhance the interface of basalt fiber (BF)/poly(vinyl chloride) (PVC) composites. polystyrene/poly(butyl acrylate) (PS/PBA)@silica JPs were synthesized by seed emulsion polymerization and three different sizing agents were prepared for BF sizing treatment. JPs with organic soft sphere and inorganic hard hemisphere enhanced the interfaces through their amphiphilicity, chemical bonding and mechanical interlock. The mechanical properties of composite with JPs sizing treated BFs performed better when there was one JPs layer modified on the interface. According to the intermitting bonding and gradient modulus theory, JPs patterned interfaces are ideal transition layers between high modulus BF and low modulus PVC.

Keywords Basalt fiber; Sizing agent; Janus particle; Composite; Interface

Citation: Liu, T. L.; Kang, P.; Wang, H.; Gao, D. L.; Xu, K.; Cai, T.; Xin, Q.; Shi, S. P.; Wang, N.; Liang, F. X. Janus particle sizing agent for interfacial enhancement of basalt fiber/poly(vinyl chloride) composites. *Chinese J. Polym. Sci.* **2025**, *43*, 1125–1133.

INTRODUCTION

Basalt fibers (BFs) derived from volcanic rocks are regarded as environmentally benign materials.[1,2] They possess the potential for application as reinforcements in polymer matrix because of their commendable mechanical and thermal performance.[3] Basalt fiber-reinforced polymer (BFRP) composites have garnered extensive attention and found various applications across various sectors, including civil and industrial construction, automotive, marine, and a viation.[4–7] However, as an inorganic fiber, BFs share similar chemical compositions and properties with glass fibers (GFs),[8] which often leads to analogous interfacial imperfections when interacting with most polymer materials. Given that interfaces play a crucial role in stress transfer between the fiber and matrix, these imperfections can significantly affect the efficacy of fiber reinforcement and, ultimately, the overall performance of the composites.[2,9] Therefore, interfacial modification has emerged as an essential strategy for the fabrication of BFRP composites.

A variety of surface treatment methods for BFs have been devised to enhance the fiber–matrix interface.[6,10–12] Among these, sizing treatment is particularly effective, as it modifies the BF surface and fabricates interfacial structures while preserving the intrinsic properties of the fibers.[13] Common BF sizing agents include polymeric coatings, coupling agents or nanomaterials. Polymeric coatings, acting as film-formers, exhibit superior surface adhesion to BFs and adjust the surface energy to align with the wettability principle of interfacial interactions.[14,15] Coupling agents form chemical bonds with both the fiber and matrix, representing another strategy for interfacial strengthening. Silane coupling agents are widely utilized for the surface modification of GFs and BFs.[16,17] The presence of nanomaterials on the fiber surface can improve its roughness, resulting in a significant expansion of the interfacial area based on mechanical interlock theory. In addition, there are some other interfacial theories proposed and studied, such as interfacial crystallization,[18,19] gradient interfacial layer,[20] intermittent bonding[21] and hierarchical structures.[22–24]

Notably, an excessively high fiber-matrix interfacial strength can precipitate brittle behavior in composites.[25] Extensive research has elucidated the correlation between the relatively weak interfacial strength and toughness of composites.[16,26,27] In comparison to strong chemical bonding, mechanical interlocking contributes more to the toughness because the energy dissipation through frictional sliding increases and the micro plastic deformation of the polymeric matrix is activated.[28] However, achieving high toughness at the expense of interfacial strength constrains the comprehen-

* Corresponding authors, E-mail: gaodl.bjhy@sinopec.com (D.L.G.)
E-mail: liangfuxin@tsinghua.edu.cn (F.X.L.)

Special Topic: Polymers at Interface
Received February 9, 2025; Accepted April 23, 2025; Published online June 18, 2025

sive performance of composites. Consequently, strategies that aim to both strengthen and toughen interfaces have consistently been at the forefront of the development trends of FRP composites.[8,29] For instance, the "chemical-physical bridges" strategy has been widely embraced, which concurrently enhances the roughness of the fiber surface and the degree of chemical bonding.[30–32] The nacre-like "brick-and-mortar" structure has been demonstrated to be an exemplary nanostructure with superior strength and toughness, and such structures can be fabricated at interfaces through layer-by-layer assembly technology.[33–36] Nevertheless, these sizing methods are often cost-prohibitive because of their laborious steps and pose challenges in the design of sizing agents, particularly for industrial-scale production. Another intriguing technique for strengthening and toughening the interfaces is the intermittent beading model, which amalgamates the advantages of intermittent bonding with bone-shaped fibers. However, the size of polymer beads limits the volume fraction of fibers, and this constraint necessitates a careful balance between the benefits of the beads and the potential reduction in the reinforcing effect of the fibers.[37,38]

In this study, we introduce a cost-effective and straightforward method for modifying the BF surface in basalt fiber/poly(vinyl chloride) (BF/PVC) composites using Janus particles (JPs) as sizing agents. JPs, characterized by their distinct physical and chemical properties in each compartment, exhibit superior interfacial activity compared to homogeneous particles.[39,40] This unique property has led to their extensive application in interfacial engineering,[41,42] with the fiber-matrix interface in composites being a promising new domain for their utilization. Herein, snowman-like JPs composed of an organic polystyrene/poly(butyl acrylate) (PS/PBA) sphere and an inorganic silica hemisphere were synthesized *via* seed emulsion polymerization. The amphiphilic nature of JPs enhances the wettability of PVC on the BF surface. Moreover, chemical bonding between JPs and BFs was achieved *via* the condensation reaction of the residual silanol groups. To further augment the size pick-up of JPs, tetraethyl orthosilicate (TEOS) and aqueous ammonia were incorporated into the sizing agent formulation. The nanoscale JPs increased the surface roughness of BFs, thereby promoting mechanical interlocking with the PVC matrix. During the processing of the BF/PVC composite, the PVC polymer chains interpenetrated the PS/PBA sphere of JPs. Consequently, the mechanical properties of the composites were improved, and simultaneous strengthening and toughening were achieved with a single layer of JPs modified at the fiber-matrix interfaces.

EXPERIMENTAL

Materials

The PS hollow spheres (HP-433) were provided by Dow Chemical. Ethylene glycol dimethacrylate (EDGMA), *n*-butyl acrylate (*n*-BA), 2,2′-azobisisobutyronitrile (AIBN), and 3-methacryloxy propyl trimethoxy silane (MPS) were purchased from Sigma Aldrich and passed through an Al_2O_3 column to remove the stabilizer before use. Sodium dodecyl sulfate (SDS) and potassium peroxydisulfate (KPS) were purchased from Sinopharm Chemical Reagent Co., Ltd. TEOS was purchased from Shanghai Macklin Biochemical Co., Ltd. Ethanol and aqueous ammonia (28 wt%) were purchased from Shanghai Titan Technology Co., Ltd. The BF without sizing agents was supplied by Tianjin Rongshi New Material Co., Ltd. PVC powder was provided by the Inner Mongolia Junzheng Group and premixed with various additives according to the laboratory-developed formulation.

Synthesis of PS/PBA Seeds and PS/PBA@silica JPs

The synthesis procedures of PS/PBA seeds and PS/PBA@silica JPs have been previously reported.[43] A PS seed water dispersion was prepared by ultrasonically dispersing 5 g of the PS hollow spheres in 93 g of deionized water. A monomer emulsion was formulated by ultrasonically dispersing 0.1 g of AIBN, 7 g of *n*-BA, 3 g of EDGMA, 0.2 g of SDS, and 60 g of deionized water. The monomer emulsion was then added to the water dispersion and mechanically stirred for 8 h at the ambient temperature. Subsequently, the mixture was heated to 80 °C for 12 h to initialize polymerization after removal of oxygen in a nitrogen atmosphere, resulting in the formation of PS/PBA seeds. For the synthesis of PS/PBA@silica JPs, 26.35 g of the aforementioned emulsion was diluted with 26.35 g of deionized water and heated to 70 °C under mechanical stirring. In parallel, 2 g of MPS was ultrasonically emulsified in 20 g of deionized water containing 0.06 g of SDS and 2 g of a 1 wt% KPS aqueous solution. The MPS monomer emulsion was slowly added to the deoxygenated PS/PBA seed emulsion for 30 min, followed by a 24-h reaction under a nitrogen atmosphere. The resulting product was isolated by centrifugation and washed several times with water and ethanol to yield PS/PBA@silica JPs.

Sizing Treatment of Chopped BF with JPs

The washed PS/PBA@silica JPs were redispersed in ethanol at specific concentrations as sizing agent-1, denoted as SA-1. TEOS was added to the JPs dispersion with a mass ratio with JPs at 1:1 to obtain sizing agent-2 and ammonia was added to sizing agent 2 with the same mass to obtain sizing agent-3, respectively denoted as SA-2 and SA-3, respectively. The chopped BFs were dried in a ventilated oven at 70 °C for 12 h and then immersed in SA-1, SA-2, and SA-3 at 60 °C for 5 min. Subsequently, the sized BFs were thoroughly dried in a vacuum oven at 120 °C overnight. For comparison, the chopped BFs without sizing treatment are denoted as SA-0.

Preparation of BF/PVC Composites

The PVC powder was dried under vacuum at 120 °C for 24 h and premixed with various additives according to a laboratory-developed formulation. The premixture was dried again under vacuum at 120 °C overnight and compounded with sized BFs to prepare BF/PVC composite samples using a micro twin screw extruder (SJZS-10B, Wuhan Ruiming Experimental Instrument Manufacturing Co., LTD) and an injection molding machine (M1200, Wuhan Qien Technology Development Co., LTD). The screw speed and feed rate were both set at 50 r/min, while the temperature profiles for the three extruder barrels were set at 175, 180, and 185 °C from the hopper to the die. Standard tensile and notched impact test bars of the BF/PVC composites were injection-molded at 180 °C, with clamping and cooling times set at 10 and 5 s respectively. The composites with BFs treated with SA-0, SA-1, SA-2, and SA-3 were denoted as PVC-BF, PVC-BF@SA-1, PVC-BF@SA-2, and PVC-BF@SA-3, respectively.

Characterization

The micro morphologies of the samples were observed by scan-

https://doi.org/10.1007/s10118-025-3366-y

ning electron microscopy (SEM, JSM-7900F, JEOL, operated at 5 kV) and transmission electron microscopy (TEM, JEM-2100Plus, JEOL, operated at 200 kV). Low-concentration ethanol dispersions of PS/PBA seeds and PS/PBA@silica JPs were dropped onto silica chips or carbon-coated copper grids and dried at room temperature for observation. The basalt fibers and fracture samples were directly attached to the specimen stage using a conductive adhesive. The size distribution of the particles was measured *via* dynamic light scattering (DLS) using a Marvin instrument (Zetasizer Nano ZS90). Fourier-transform infrared spectroscopy (FTIR, Invenio R, Bruke) was used to analyze the chemical structures of PS/PBA seeds and PS/PBA@silica JPs within the wavenumber range of 400–4000 cm^{-1}. The surface energies of different sized BFs were calculated through contact angle measurements with polar (water) and nonpolar (*n*-hexadecane) probe liquids using a contact angle measurement system (OCA25, Dataphysics). Tensile tests and three-point bend tests were performed using a universal testing machine (UTM-1432, Chengde Jinjian Instrument Co., LTD) at room temperature. The notched Izod impact performance of the composite was tested using an impact tester (XJUD-5.5, Chengde Jinjian Instrument Co., LTD) at room temperature with a pendulum energy of 5.5 J. The modulus of the interfacial region between BF and PVC was investigated using atomic force microscopy (AFM, Icon, Bruker) in the PeakForce quantitative nanomechanical (QNM) mode. The RTESPA 300 probe was used with a cantilever spring constant of 40 N/m. The scanning rate was 0.5 Hz, the number of scanning points was 512 × 512, and scanning area size was 10 μm.

RESULTS AND DISCUSSION

Synthesis and Characterization of PS/PBA@silica JPs

The synthesis process of PS/PBA@silica JPs is shown in Fig. 1(a). Commercial PS hollow spheres were utilized as seeds and swollen by *n*-BA and EDGMA. A crosslinked PBA network interpenetrated PS after polymerization, resulting in a wrinkled morphology and a thicker shell compared to the original PS hollow spheres, as evidenced by SEM and TEM (Figs. 1b and 1c). These PS/PBA seeds were subsequently utilized for the synthesis of JPs *via* polymerization-induced phase separation, with MPS serving as the monomer owing to its dual reactive functionalities. The polymerization of MPS led to a significant decrease in its solubility in PS, and upon hydrolysis-condensation reactions of siloxane groups, a silica hemisphere was achieved. Thus, a snowman-like Janus structure with a PS/PBA organic sphere and a silica inorganic hemisphere was obtained (Fig. 1d).

Energy dispersive spectrometry (EDS) mapping revealed that O and Si were predominantly concentrated in the silica hemisphere of the JPs (Fig. 2a). The average diameter of JPs further increased to 608.5 nm, with a broadened size distribution (Fig. 2b). In the FTIR spectra (Fig. 2c), the characteristic adsorption peaks at 1735, 1166 and 2954 cm^{-1}, corresponding to the C=O, C−O, and C−H groups of the ester bonds, respectively, confirmed the successful incorporation of acrylic monomers into the PS hollow spheres. Additionally, the presence of condensed siloxane (1090 cm^{-1}) and uncondensed silanol (3305 cm^{-1}) stretching signals in PS/PBA@silica JPs indicated that the hemisphere separated from PS/PBA seeds exhibited a silica-like chemical structure. Notably, residual silanol groups were observed on the silica hemisphere, suggesting that JPs could participate in subsequent reactions.

Sizing Treatment of BFs with JPs

Unsized BFs were designated as SA-0. BFs treated solely with JPs, JPs combined with TEOS, and JPs combined with TEOS and ammonia are denoted as SA-1, SA-2, and SA-3, respectively. During the sizing process, JPs interacted with the BF surface and were modified on it (Fig. 3a). The size pick-up percentage, defined as the mass ratio of the grafted sizing components to pristine BF, serves as a critical indicator for evaluating the grafting efficiency of JPs. As shown in Fig. 3(b), only the JPs system (SA-1) exhibited a baseline pick-up of 1.9%, which increased to 2.4% with TEOS incorporation in SA-2. This 26.3% enhancement originates from the *in situ* formation of a siloxane network *via* TEOS hydrolysis-condensation. The subsequent addition of ammonia

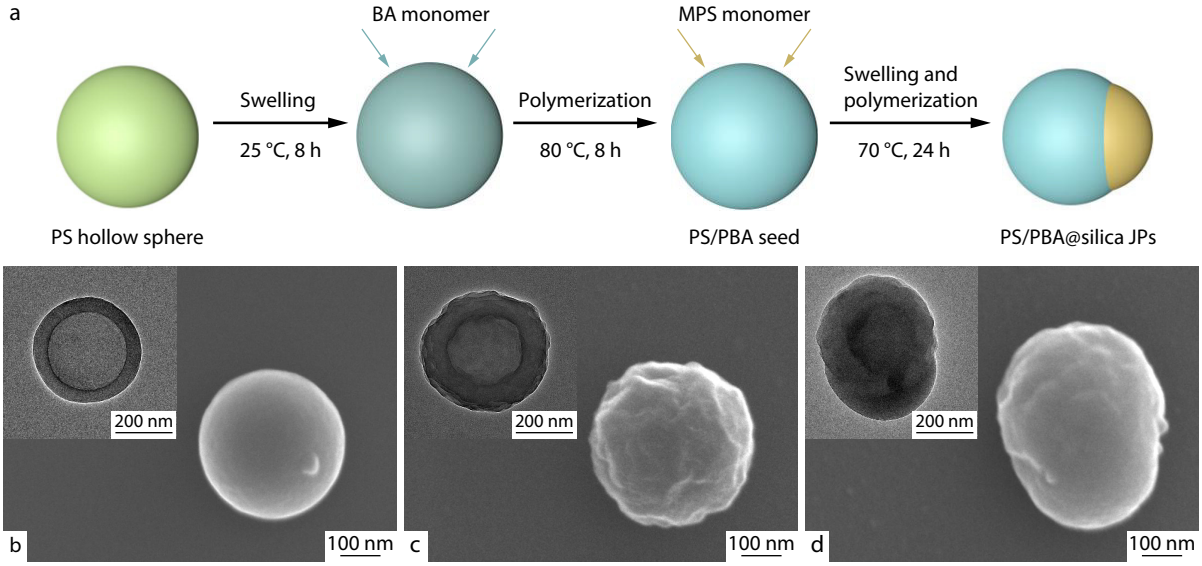

Fig. 1 Synthesis and morphological characterization of JPs: (a) schematic diagram of synthesis of PS/PBA@silica JPs; (b–d) SEM and inset TEM images of (b) PS hollow sphere , (c) PS/PBA seed , and (d) PS/PBA@silica JPs.

https://doi.org/10.1007/s10118-025-3366-y

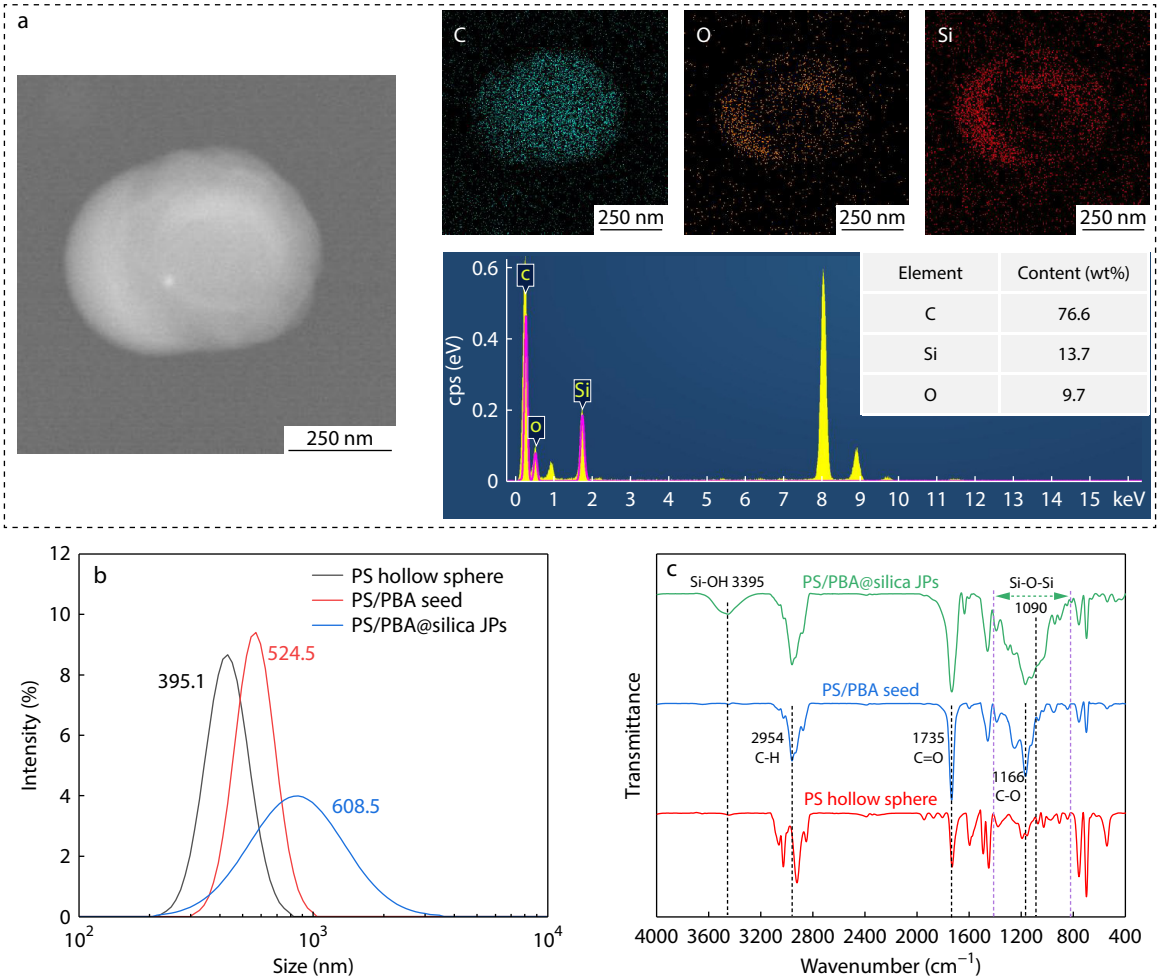

Fig. 2 Composition and microstructure analysis of as-synthesized JPs: (a) EDS element mapping images of PS/PBA@silica JPs; (b) DLS diagram and (c) FTIR spectra of the PS hollow sphere, PS/PBA seed and PS/PBA@silica JPs.

(SA-3) further elevated the pick-up to 3.3%, representing a 37.5% increase over SA-2, confirming that alkaline catalysis promotes silanol group reactivity and polycondensation efficiency. Crucially, the low intrinsic grafting affinity of JPs alone (SA-1) results in discontinuous interfacial deposition, and incomplete TEOS conversion under non-catalytic conditions (SA-2) leaves unreacted intermediates, which may compromise the interfacial properties.

The surface energy of BF modified with JPs was quantitatively assessed through contact angle measurements using polar (water) and nonpolar (n-hexadecane) probe liquids. The polar surface energy (γ^p) and dispersive surface energy (γ^d) of sized BFs were calculated using Eq. (1).

$$\gamma_l(1+\cos\theta) = 2\sqrt{\gamma^p\gamma_l^p} + 2\sqrt{\gamma^d\gamma_l^d} \quad (1)$$

where θ is the static contact angle and γ_l, γ_l^p and γ_l^d are the surface energy and its polar and dispersive components of the probe liquids, respectively. As shown in Fig. 3(c), the unsized BF exhibited high surface energy dominated by polar component ($\gamma^p = 40.8$ mJ/m^2), and JPs modification significantly altered this profile, reducing γ^p by 24.0% while increasing γ^d by 14.2%. The polarity reversal correlates with the chemical affinity between the JP ester groups and PVC matrix, promoting interfacial wetting in the composite. A monotonic increase in polar liquid contact angles from 33.9° (SA-1) to 56.9° (SA-3) paralleled the size pick-up progression, whereas the nonpolar liquid contact angles reached a minimum (17.2°) at SA-2. The resultant γ^d values followed a nonlinear trend, with SA-3 showing 6.8% lower than that of SA-2. These results can be explained by the morphology of the BF surfaces with different numbers of JPs modified.

Figs. 4(a)–4(d) present the progressive morphological evolution of BFs under different sizing treatments. Compared to pristine BFs (Fig. 4a), the incorporation of JPs significantly enhanced the surface roughness of BFs. As the size pick-up increased from SA-1 to SA-3, more JPs were grafted onto the BF surface and formed a rough particulate layer. As a result, smooth fibre surfaces were rarely observed in SEM images. In SA-1 and SA-2, most JPs contacted directly with the fibre surface (Figs. 4b and 4c). In such case, a higher JP grafting efficiency means the modified surface behaved more like particles than fibres. This morphological evolution confirmed the continuous changes of the contact angles and surface energies between SA-0, SA-1 and SA-2. In contrast, under the catalytic effect of ammonia in SA-3, JPs aggregated into clusters on the fibre surface (Fig. 4d). It demonstrated that the rapid hydrolysis-condensation reactions facilitated the formation of chemical bonds between JPs. Since the fibre surface were fully covered by JPs, the surface energy remained stabled de-

https://doi.org/10.1007/s10118-025-3366-y

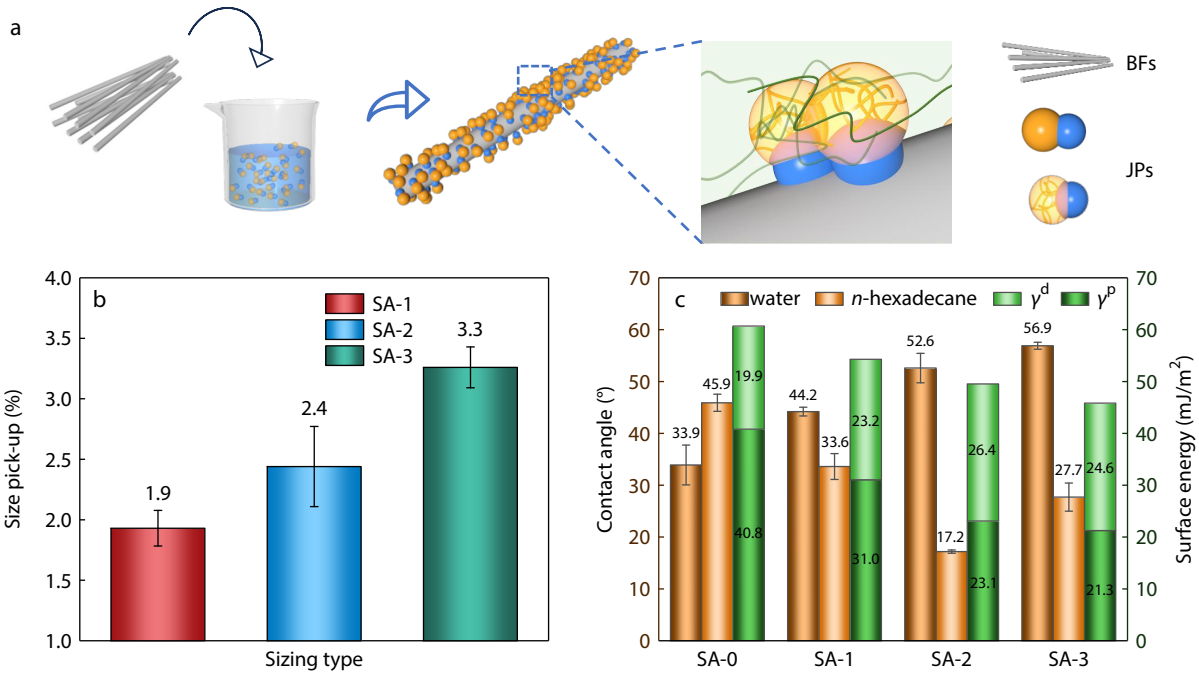

Fig. 3 Sizing treatment of BFs with JPs: (a) Schematic diagram of BF sizing treatment with JPs; (b) Size pick-ups, (c) contact angles and surface energies of BFs with above different sizing treatments.

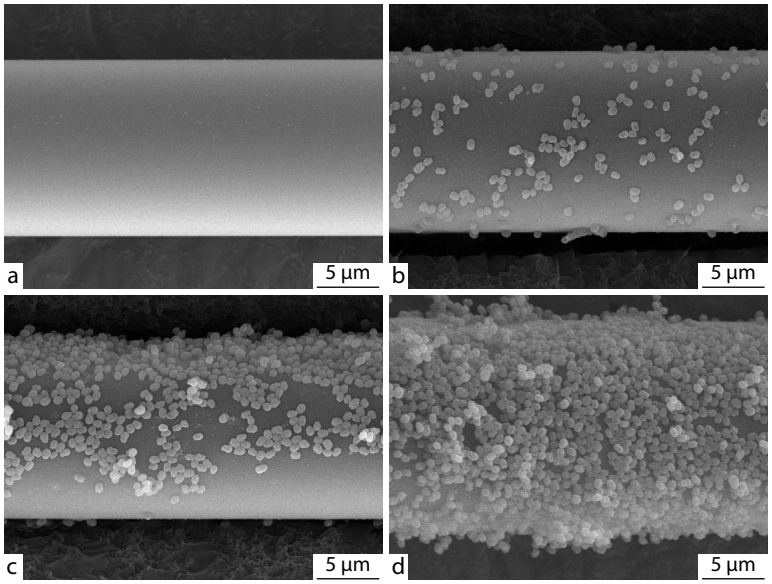

Fig. 4 SEM images of the BF surface with different sizing treatments: (a) SA-0, (b) SA-1, (c) SA-2, and (d) SA-3.

spite increased JP loading. Due to the roughness significantly enhanced by the clusters of JPs, the contact angles of water and n-hexadecane both increased on BF surface in SA-3, causing reduction of dispersive surface energy that deviated from the previous trend.

Mechanical Properties of BF/PVC Composites

Tensile, bending, and notched impact tests were conducted on BF/PVC composites to elucidate the relationship between the modification of interfaces with JPs and the mechanical properties of the composite (Figs. 5a–5f). After the sizing treatment with PS/PBA@silica JPs, the tensile modulus exhibited no significant change, whereas the flexural modulus increased markedly in SA-1 and SA-3 by 6.2% and 8.7%, respectively. The amphiphilic nature of JPs enhanced the wettability of PVC on the BF surface, thereby improving the interfacial adherence and achieving more effective mechanical interlocking. When only TEOS was incorporated into the dispersion of JPs, the concentration of silanol groups increased, while their reactivity remained unchanged. The unreacted TEOS residues on the BF surface compromised interfacial contact, resulting in an inferior flexural modulus. In SA-3, ammonia catalyzed the formation of Si-O-Si bonds. JPs were grafted onto the BF surface through rigid chemical structures and TEOS in SA-3 exhibited a higher degree of reaction completeness compared to SA-2. Conse-

https://doi.org/10.1007/s10118-025-3366-y

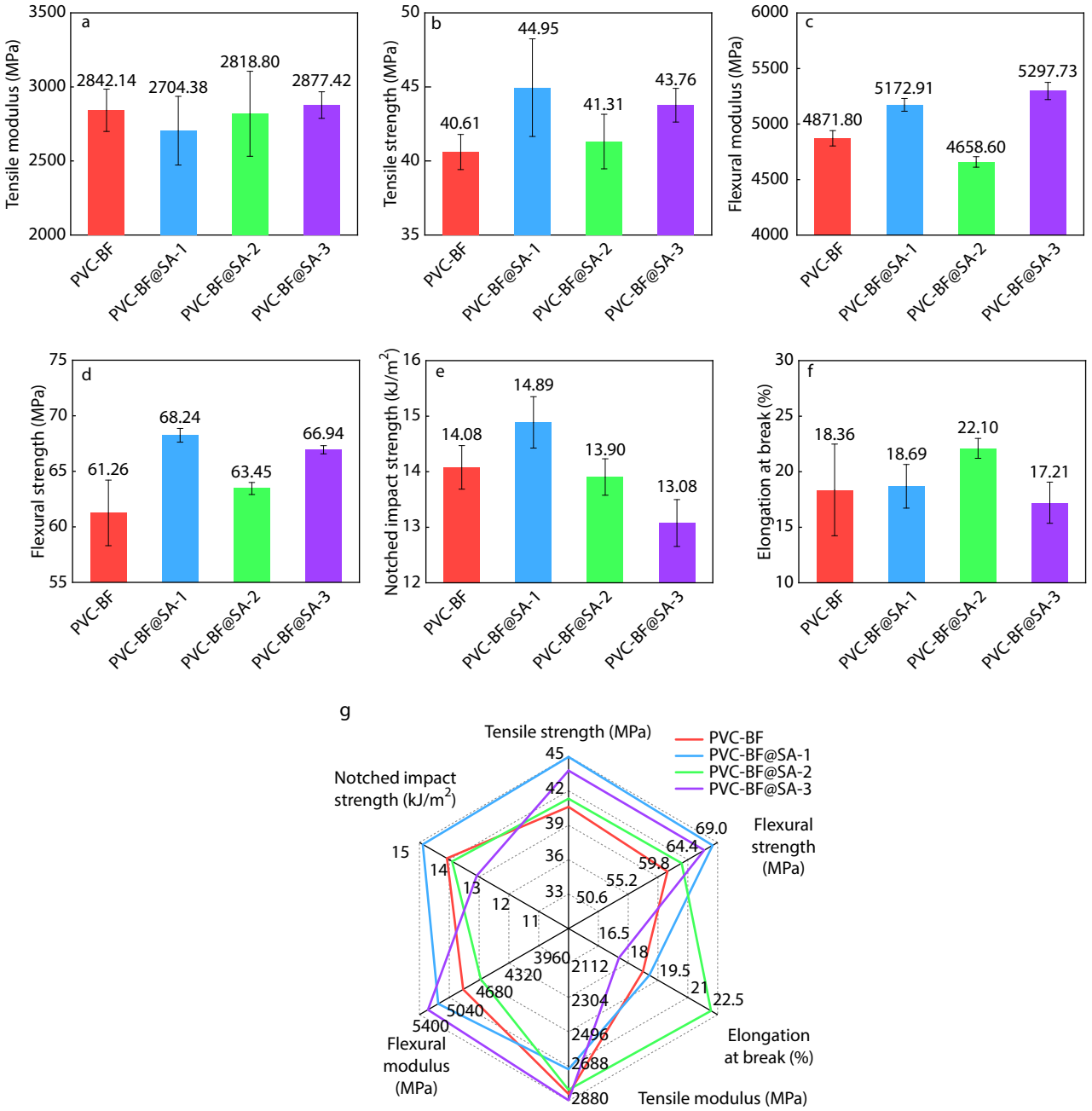

Fig. 5 Mechanical properties of the BF/PVC composites with different sizing treatments: (a) tensile modulus, (b) tensile strength, (c) flexural modulus, (d) flexural strength, (e) notched impact strength and (f) elongation at break of different composites, (g) represented as radar plot showing averages for each mechanical property.

quently, the flexural modulus of the PVC-BF@SA-3 composite reached 5297.73 MPa, which is 19.7% higher than that of PVC-BF@SA-2 without ammonia. Notably, the tensile and flexural strengths of PVC-BF@SA-1 were superior to those of PVC-BF@SA-3. This inferior performance of PVC-BF@SA-3 can be attributed to the clusters of JPs on the fiber surface. These structures act as defects at the interfaces during composite failure.

Notched impact strength is a crucial parameter for evaluating the toughness of composites. Among the three JPs sizing treatment systems, PVC-BF@SA-1 performed best, with a 5.8% enhancement in the notched impact strength. The interfaces modified by JPs are capable of effectively transferring the impact stress to the BF, which has a higher modulus. Simultaneously, these interfaces can absorb a portion of the impact energy through minor plastic deformation at the interface. In contrast, PVC-BF@SA-3, with a higher modulus, underwent brittle fracture upon impact owing to its rigid interfaces, characterized by an abundance of chemical bonds between the JPs. The poor elongation at break of PVC-BF@SA-3 further supported the notion that rigid interfaces are prone to brittle failure. In contrast, PVC-BF@SA-2 demonstrated a lower modulus and strength, but higher elongation at break. The inter-

https://doi.org/10.1007/s10118-025-3366-y

faces with JPs and TEOS exhibited notable deformability under tensile stress, but they retained sufficient mechanical integrity to maintain structural coherence. This enabled the composite to deform extensively and adsorb external energy, thereby delaying the onset of fracture.

These results indicate that JPs with one ideal particle layer arrangement on the fiber surface can optimize the comprehensive performance of the composite (Fig. 5g). The snowman-like PS/PBA@silica JPs on the fiber formed a patterned surface with distinct mechanical and chemical properties.[44] The silica hemisphere, with its high modulus, provided strong chemical bonding with inorganic BFs, while PS/PBA seeds infiltrated with PVC allowed for microscale deformation at the interface to dissipate external energy. According to the intermitting bonding theory[21] and gradient modulus theory[20], an interface with a rigid-strong/soft-tough pattern can serve as an ideal transition layer between high-modulus BF and low-modulus PVC.

Microscopic Characterization of BF/PVC Composites

To elucidate the mechanisms by which the interface reinforcement structures impart different mechanical properties, the tensile-fractured surfaces of the different samples were further observed using SEM (Figs. 6a–6d). The reduced fiber pull-out length suggests a more robust interfacial bonding, particularly when comparing PVC-BF@SA-3 with PVC-BF. The JPs with dissimilar chemical properties on their opposite sides improved the interfacial strength. Moreover, incorporation of TEOS under alkaline conditions further augmented this effect. Deformation of the PVC matrix was observed across all tensile-fractured surfaces of the composites, with the exception of PVC-BF@SA-3. This observation can be attributed to the rigid interfaces with high modulus, which effectively anchored the ductile polymer matrix to the hard inorganic fiber. Consequently, PVC-BF@SA-3 exhibited a more brittle behavior than the other composites, characterized by a higher modulus and a lower elongation at break. In contrast, PVC-BF@SA-1 with a single layer of JPs at the fiber–matrix interface (Fig. 6b) achieved an optimal balance between strength and toughness. This composite demonstrated a shorter fiber pull-out length than PVC-BF, while still maintaining the deformability of the matrix under tensile stress.

The interfacial phases of PVC-BF and PVC-BF@SA-1 were quantitatively characterized using AFM in the PeakForce QNM mode. As shown in Fig. 7, compared with the bare interface in PVC-BF, the JP-modified interface exhibited a gradient modulus layer between the low-modulus PVC matrix and high-modulus BF, which represents the interfacial phase. The modulus increased suddenly at the interface in the PVC-BF owing to the weak interfacial adhesion. This stepwise transition in the modulus between BF and PVC caused a poor stress transfer capacity from the matrix to the reinforcement. In contrast, in the PVC-BF@SA-1 composite, the modulus increased gradually with an interfacial phase thickness of approximately 271 nm, which is of the same order of magnitude as the size of JPs. The snowman-like JPs, integrating a rigid silica hemisphere and a soft polymer sphere, established a moderate modulus bridge between the modulus gap of the fiber and the matrix. Consequently, the single layer of JPs modified at the interface optimizes the interfacial stress transfer efficiency.

CONCLUSIONS

In this study, specifically designed JPs were synthesized to enhance the interfaces of the BF/PVC composite, serving as sizing agents. The silica hemispheres of JPs reacted with silanol groups on BF, while the PVC matrix infiltrated their PS/PBA portion, thus creating better interfaces. By enhancing both the resin wettability to the fiber and the mechanical interlock of the nanoparticle modification, the interfacial strength and toughness were simultaneously improved. To further increase size pick-up, TEOS and ammonia were incorporated into the JPs sizing agent. This led to a higher quantity of JPs being chemically grafted onto the BF surfaces, with some clustering of JPs. The WCA increased from 68° to 105° after the sizing treatment with TEOS and ammonia. However, the higher quantity of rigid Si—O—Si bonds resulted in an increased modulus and reduced ductility, causing the composite to exhibit brittleness during stretching and impact

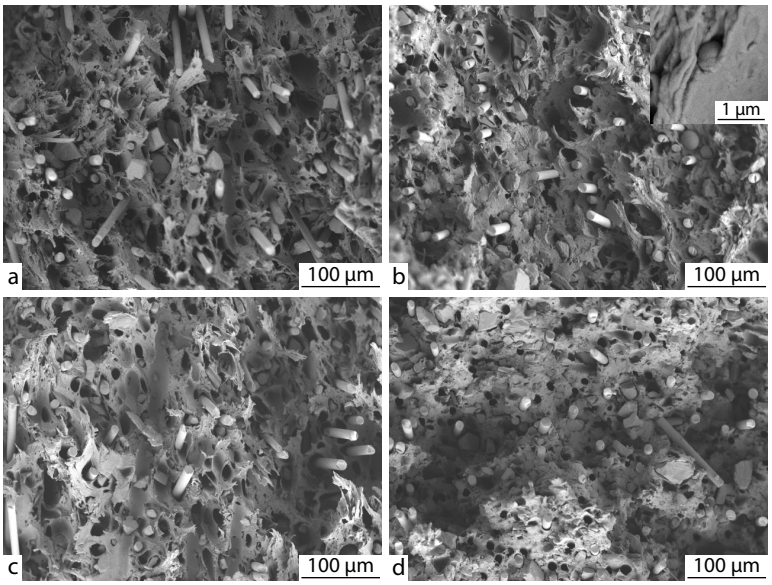

Fig. 6 SEM morphologies of tensile-fractured surfaces of (a) PVC/BF, (b) PVC/BF@SA-1, with JP in PVC matrix near the interface, (c) PVC/BF@SA-2 and (d) PVC/BF@SA-3.

https://doi.org/10.1007/s10118-025-3366-y

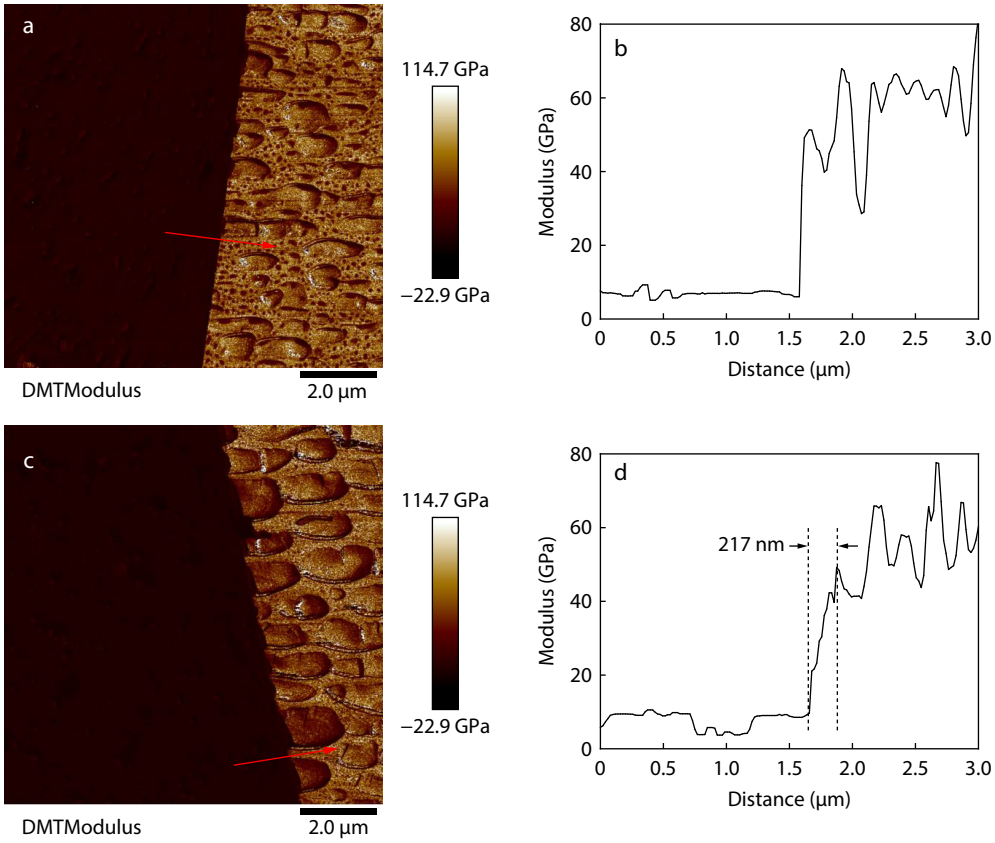

Fig. 7 (a, c) AFM images and (b, d) modulus curves for the interfacial phase: (a, b) PVC-BF and (c, d) PVC-BF@SA-1.

tests.

The characterization of the mechanical properties of BF/PVC composites revealed that different sizing treatments significantly affected the interface. Among the composites tested, PVC-BF@SA-2 exhibited the highest modulus and lowest ductility, whereas PVC-BF@SA-3 exhibited the opposite behavior. Overall, PVC-BF@SA-1 exhibited excellent performance when single-layer JPs were grafted onto the fiber surface. Compared with the non-sized PVC/BF composite, PVC-BF@SA-1 demonstrated improvements in flexural modulus (6.2%), flexural strength (11.4%), and notched impact strength (5.8%). The interfacial phase with a gradient modulus constructed by single-layer JPs contributed to the simultaneous enhancement of interfacial strength and toughness.

In summary, a novel interfacial modification methodology using JPs was implemented and validated. Further development will be pursued for better sizing treatment technologies and more effective interfacial models.

Conflict of Interests

The authors declare no interest conflict.

Data Availability Statement

The data that support the findings of this study are available from the corresponding author upon reasonable request. The author's contact information: gaodl.bjhy@sinopec.com (D.L.G.), liangfuxin@tsinghua.edu.cn (F.X.L).

ACKNOWLEDGMENTS

This work was financially supported by the National Natural Science Foundation of China (Nos. U22A20252 and 52173076), the Beijing Natural Science Foundation (Nos. Z240030 and L248023), and the Liaoning Province Key Research and Development Project (No. 2024JH2/102400046).

REFERENCES

1 Fiore, V.; Scalici, T.; Di Bella, G.; Valenza, A. A review on basalt fibre and its composites. *Compos. Part B Eng.* **2015**, *74*, 74–94.
2 Chen, C.; Ding, Y.; Wang, X.; Bao, L. Recent advances to engineer tough basalt fiber reinforced composites: a review. *Polym. Compos.* **2024**, *45*, 12559–12574.
3 Jagadeesh, P.; Rangappa, S. M.; Siengchin, S. Basalt fibers: an environmentally acceptable and sustainable green material for polymer composites. *Constr. Build. Mater.* **2024**, *436*, 136834.
4 Monaldo, E.; Nerilli, F.; Vairo, G. Basalt-based fiber-reinforced materials and structural applications in civil engineering. *Compos. Struct.* **2019**, *214*, 246–263.
5 Jamshaid, H.; Mishra, R. A Green material from rock: basalt fiber – a review. *J. Text. Inst.* **2016**, *107*, 923–937.
6 K.V., B.; Shirvanimoghaddam, K.; Rajan, G. S.; Ellis, A. V.; Naebe, M. Surface treatment of basalt fiber for use in automotive composites. *Mater. Today Chem.* **2020**, *17*, 100334.
7 Sun, L.; Wang, C.; Zhang, C.; Yang, Z.; Li, C.; Qiao, P. Experimental investigation on the bond performance of sea sand coral concrete with frp bar reinforcement for marine environments.

Adv. Struct. Eng. **2023**, *26*, 533–546.
8 Wu, Q.; Deng, H.; Xiao, B.; Ye, Z.; Zhu, J. New simple strategy for improving interfacial adhesion of basalt fiber composites by adhering bio-based *β*-cyclodextrin on fiber. *Compos. Commun.* **2024**, *45*, 101805.
9 Wang, J.; Marashizadeh, P.; Weng, B.; Larson, P.; Altan, M. C.; Liu, Y. Synthesis, characterization, and modeling of aligned zno nanowire-enhanced carbon-fiber-reinforced composites. *Materials* **2022**, *15*, 2618.
10 Hou, X.; Yao, S.; Wang, Z.; Fang, C.; Li, T. Enhancement of the mechanical properties of polylactic acid/basalt fiber composites *via in-situ* assembling silica nanospheres on the interface. *J. Mater. Sci. Technol.* **2021**, *84*, 182–190.
11 Wang, Z. T. Mechanical properties of basalt fiber improved by starch phosphates sizing agent. *Appl. Surf. Sci.* **2020**, *521*, 146196.
12 Ning, N.; Wang, M.; Zhou, G.; Qiu, Y.; Wei, Y. Effect of polymer nanoparticle morphology on fracture toughness enhancement of carbon fiber reinforced epoxy composites. *Compos. Part B Eng.* **2022**, *234*, 109749.
13 Yang, A.; He, P.; Li, G.; Ye, J.; Huang, Y.; Han, R.; Zhang, S. Improving the curing reactivity, interfacial strength, thermal and mechanical properties of phthalonitrile resin/basalt fiber composites by reactive organic coating. *Colloids Surf. Physicochem. Eng. Asp.* **2024**, *703*, 135335.
14 Liu, W.; Zhu, Y.; Qian, C.; Dai, H.; Fu, Y.; Dong, Y. Interfacial modification between glass fiber and polypropylene using a novel waterborne amphiphilic sizing agent. *Compos. Part B Eng.* **2022**, *241*, 110029.
15 Jia, H.; Liu, C.; Qiao, Y.; Zhang, Y.; Fan, K.; Zhang, M.; Jian, X. Highly enhancing the interfacial and mechanical properties of basalt fiber/poly(phthalazinone ether nitrile ketone) composite by thermoplastic sizing agents with different structures. *Polymers* **2022**, *14*, 2947.
16 Jia, H. Enhanced interfacial and mechanical properties of basalt fiber reinforced poly(aryl ether nitrile ketone) composites by amino-silane coupling agents. *Polymer* **2021**, *230*, 124028.
17 Thomason, J. L. Glass fibre sizing: a review. *Compos. Part Appl. Sci. Manuf.* **2019**, *127*, 105619.
18 Luo, G.; Li, W.; Liang, W.; Liu, G.; Ma, Y.; Niu, Y.; Li, G. Coupling Effects of glass fiber treatment and matrix modification on the interfacial microstructures and the enhanced mechanical properties of glass fiber/polypropylene composites. *Compos. Part B Eng.* **2017**, *111*, 190–199.
19 Allen, K. A.; Kearney, L. T.; Gupta, S.; Ghossein, H.; Keum, J. K.; Damron, J. T.; Humphrey, H. E.; Vaidya, U.; Naskar, A. K. Understanding interfacial crystallization dynamics on carbon fiber reinforced polypropylene composite manufacturing. *Compos. Part B Eng.* **2025**, *291*, 112027.
20 Feng, P.; Ma, L.; Zhou, X.; Li, M.; Zhang, Q.; Zhang, M.; Liu, X.; Jian, X.; Xu, J. Constructing a gradient modulus interface layer on the surface of carbon fibers to enhance the mechanical properties of carbon fiber/epoxy composites at different temperatures. *Compos. Part B Eng.* **2024**, *271*, 111190.
21 Atkins, A. G. Intermittent bonding for high toughness/ high strength composites. *J. Mater. Sci.* **1975**, *10*, 819–832.
22 Gupta, S.; Sohail, T.; Checa, M.; Rohewal, S. S.; Toomey, M. D.; Kanbargi, N.; Damron, J. T.; Collins, L.; Kearney, L. T.; Naskar, A. K.; Bowland, C. C. Enhancing composite toughness through hierarchical interphase formation. *Adv. Sci.* **2024**, *11*, 2305642.
23 Tian, H.; Fan, W.; Ge, S.; Xia, C.; Liu, Y.; Wang, H.; Wang, S. Nanofiber-sheathed structure for enhancing interfacial properties of basalt fiber-reinforced composites. *Compos. Commun.* **2021**, *23*, 100589.
24 Kumar, S.; Graninger, G.; Hawkins, S. C.; Falzon, B. G. A Nanostructured cellulose-based interphase layer to enhance the mechanical performance of glass fiber-reinforced polymer composites. *Compos. Part Appl. Sci. Manuf.* **2021**, *148*, 106475.
25 Zhong, K.; Zhou, J.; Zhao, C.; Yun, K.; Qi, L. Effect of interfacial transition layer with cnts on fracture toughness and failure mode of carbon fiber reinforced aluminum matrix composites. *Compos. Part Appl. Sci. Manuf.* **2022**, *163*, 107201.
26 Jiang, L.; Zhou, Y.; Jin, F. Design of short fiber-reinforced thermoplastic composites: a review. *Polym. Compos.* **2022**, *43*, 4835–4847.
27 Klingler, A.; He, Q.; Wetzel, B.; Allen, T.; Ye, L.; Breuer, U. Low velocity impact resistance of thin and toughened carbon fibre reinforced epoxy. *Compos. Sci. Technol.* **2022**, *230*, 109362.
28 Mishnaevsky, L. Nanostructured interfaces for enhancing mechanical properties of composites: computational micromechanical studies. *Compos. Part B Eng.* **2015**, *68*, 75–84.
29 Wu, Z.; Cui, H.; Chen, L.; Jiang, D.; Weng, L.; Ma, Y.; Li, X.; Zhang, X.; Liu, H.; Wang, N.; Zhang, J.; Ma, Y.; Zhang, M.; Huang, Y.; Guo, Z. Interfacially reinforced unsaturated polyester carbon fiber composites with a vinyl ester-carbon nanotubes sizing agent. *Compos. Sci. Technol.* **2018**, *164*, 195–203.
30 Zhao, Y.; Zhang, S.; Xu, Q.; Wang, K.; Xu, Z.; Long, T.; Jin, T.; Jiang, M.; Liu, P. Synergistic enhancement of mechanical and thermal properties in basalt fiber reinforced composites through nanotube and graphene bridging structure: a multi-scale simulation. *Compos. Part B Eng.* **2025**, *297*, 112289.
31 Sun, Z. Mechanical enhancement of carbon fiber-reinforced polymers: from interfacial regulating strategies to advanced processing technologies. *Prog. Mater. Sci.* **2024**, *142*, 101221.
32 Mahmood, H.; Tripathi, M.; Pugno, N.; Pegoretti, A. Enhancement of interfacial adhesion in glass fiber/epoxy composites by electrophoretic deposition of graphene oxide on glass fibers. *Compos. Sci. Technol.* **2016**, *126*, 149–157.
33 De Luca, F.; Sernicola, G.; Shaffer, M. S. P.; Bismarck, A. "Brick-and-mortar" nanostructured interphase for glass-fiber-reinforced polymer composites. *ACS Appl. Mater. Interfaces* **2018**, *10*, 7352–7361.
34 Wu, Q.; Yang, X.; Wan, Q.; Zhao, R.; He, J.; Zhu, J. Layer-by-layer assembled nacre-like polyether amine/go hierarchical structure on carbon fiber surface toward composites with excellent interfacial strength and toughness. *Compos. Sci. Technol.* **2020**, *198*, 108296.
35 Yu, J.; Chen, S.; Huang, H.; Yu, F.; Yao, P.; Fan, Z.; Yang, H.; Liu, H.; Zhu, C.; Xu, J. A universal strategy for rapid and scalable surface modification of ultra high molecular weight polyethylene fiber. *Compos. Struct.* **2024**, *334*, 117935.
36 Feng, P.; Ma, L.; Quan, Y.; Liu, X.; Zhou, X.; Chen, T.; Jian, X.; Xu, J. Layer-by-layer assembly of a novel biomimetic fish scale structure onto carbon fiber surface *via* thiol-ene click chemistry to enhance high-temperature resistance and functionality of carbon fiber/epoxy composites. *J. Colloid Interface Sci.* **2025**, *686*, 75–87.
37 Greenfeld, I.; Zhang, W.; Sui, X.; Wagner, H. D. Intermittent beading in fiber composites. *Compos. Sci. Technol.* **2018**, *160*, 21–31.
38 Xu, M.; An, B. Plastic deformation of polymer matrix composites reinforced with beaded fibers. *Int. J. Solids Struct.* **2022**, *256*, 111985.
39 De Gennes, P. G. Soft matter. *Rev. Mod. Phys.* **1992**, *64*, 645–648.
40 Binks, B. P.; Fletcher, P. D. I. Particles adsorbed at the oil–water interface: a theoretical comparison between spheres of uniform wettability and "janus" particles. *Langmuir* **2001**, *17*, 4708–4710.
41 Agrawal, G.; Agrawal, R. Janus nanoparticles: recent advances in their interfacial and biomedical applications. *ACS Appl. Nano Mater.* **2019**, *2*, 1738–1757.
42 Liang, F.; Liu, B.; Cao, Z.; Yang, Z. Janus colloids toward interfacial engineering. *Langmuir* **2018**, *34*, 4123–4131.
43 He, H.; Liang, F. Engineering polymer blends with controllable interfacial location of janus particles as compatibilizers. *Chem. Mater.* **2022**, *34*, 3806–3818.
44 Kirillova, A.; Ionov, L.; Roisman, I. V.; Synytska, A. Hybrid hairy janus particles for anti-icing and de-icing surfaces: synergism of properties and effects. *Chem. Mater.* **2016**, *28*, 6995–7005.

https://doi.org/10.1007/s10118-025-3366-y